Electronic Supplementary Information

for

Quantitative analysis of air-oxidation reactions of thiolate-protected gold nanoclusters

Wataru Suzuki,[a†] Ryo Takahata,[a,b] Yoshiyuki Mizuhata,[a,b,c] Norihiro Tokitoh,[a,b,c]

Songlin Xue[d] and Toshiharu Teranishi*[a,b]

[a] *Institute for Chemical Research, Kyoto University, Gokasho, Uji, Kyoto 611-0011, Japan*

[b] *Graduate School of Science, Kyoto University, Gokasho, Uji, Kyoto 611-0011, Japan*

[c] *Integrated Research Consortium on Chemical Sciences, Uji, Kyoto 611-0011, Japan*

[d] *School of Chemistry and Chemical Engineering, Jiangsu University, 301 Xuefu Road, Zhenjiang 212013, China*

[†] *Present address: University of Hyogo, Himeji, Hyogo 671-2280, Japan*

E-mail: teranisi@scl.kyoto-u.ac.jp; Fax: +81-774-38-3121

Contents

Experimental Section

Materials

General. Organic solvents, starting materials and reagents for synthesis were purchased from commercial sources and used without further purification. **TOA$^+$[Au$_{25}$(SC$_2$Ph)$_{18}$]$^-$** (SC$_2$Ph = phenylethanethiolate, TOA$^+$ = tetraoctylammonium),[1] and **TOA$^+$[Au$_{23}$(SCy)$_{16}$]$^-$** (SCy = cyclohexanethiolate)[2] were synthesized according to the previous reports.

Synthesis

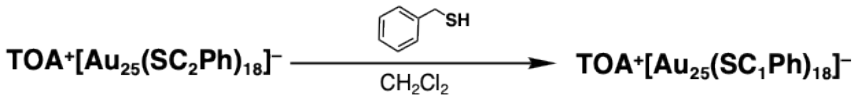

TOA$^+$[Au$_{25}$(SC$_1$Ph)$_{18}$]$^-$. Benzyl mercaptan (**PhC$_1$SH**, 1.8 mL, 1.9 g, 15 mmol) was added to a solution of **TOA$^+$[Au$_{25}$(SC$_2$Ph)$_{18}$]$^-$** (30.0 mg, 3.82 μmol) in CH_2Cl_2 (6 mL) and the solution was stirred for 1 h at 313 K. Progress of the reaction was monitored using UV–vis spectroscopy. After the reaction, MeOH (~40 mL) was added and the mixture was centrifuged (9600 *g*, 10 min) to precipitate the targeted clusters. The precipitate was collected and washed with MeOH to afford **TOA$^+$[Au$_{25}$(SC$_1$Ph)$_{18}$]$^-$** (20.0 mg, 2.63 μmol) in 69% yield.

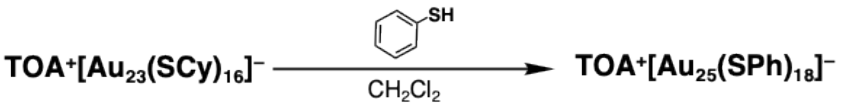

TOA$^+$[Au$_{25}$(SPh)$_{18}$]$^-$. Benzenethiol (**PhSH**, 0.80 mL, 0.86 g, 7.8 mmol) was added to the solution of **TOA$^+$[Au$_{23}$(SCy)$_{16}$]$^-$** (18.7 mg, 2.73 μmol) in CH_2Cl_2 (4 mL) and the solution was stirred overnight at 298 K. Progress of the reaction was monitored using UV–vis spectroscopy. After the reaction, MeOH (~25 mL) was added and the mixture was centrifuged (9600 *g*, 5 min) to precipitate impurities. The supernatant was concentrated to a small volume and centrifuged (9600 *g*, 10 min) to precipitate the targeted clusters. The precipitate was collected and washed with MeOH to afford **TOA$^+$[Au$_{25}$(SPh)$_{18}$]$^-$** (10.4 mg, 1.41 μmol) in 56% yield.

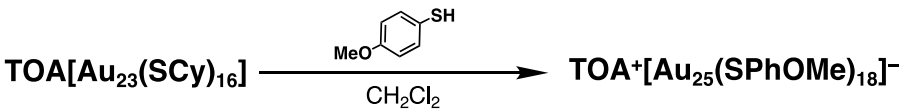

TOA$^+$[Au$_{25}$(SPhOMe)$_{18}$]$^-$. 4-Methoxybenzenethiol (**MeOPhSH**, 0.75 mL, 0.85 g, 6.1 mmol) was added to the solution of **TOA$^+$[Au$_{23}$(SCy)$_{16}$]$^-$** (17.5 mg, 2.56 μmol) in CH_2Cl_2 (3 mL) and

the solution was stirred for 1.5 h at 313 K. Progress of the reaction was monitored using UV–vis spectroscopy. After the reaction, MeOH (~25 mL) was added and the mixture was centrifuged (9600 *g*, 5 min) to precipitate impurities. The supernatant was concentrated to a small volume and centrifuged (9600 *g*, 10 min) to precipitate the targeted clusters. The precipitate was collected and washed with MeOH to afford **$TOA^+[Au_{25}(SPhOMe)_{18}]^-$** (7.5 mg, 0.94 μmol) in 37% yield.

Measurements

X-ray Crystallography. Single crystals of **$TOA^+[Au_{25}(SPh)_{18}]^-$** were grown by recrystallization with a vapour diffusion of EtOH into the toluene solution of **$TOA^+[Au_{25}(SPh)_{18}]^-$**. The single crystals were mounted using a mounting loop. The intensity data were collected at 90 K on a Bruker D8 VENTURE system (PHOTONIII 14 with IμS Diamond) using Mo Kα radiation (λ = 0.71073 Å). The structure was solved using SHELXT-2018/2[3] and refined by least-squares calculations on F^2 for all reflections (SHELXL-2019/3).[4] All non-hydrogen atoms were refined anisotropically. All calculations were performed using Yadokari-XG 2011 software package[5] and Olex2-1.5.[6] In the CheckCIF report, several level B alerts are noted as below, which are derived from the severe disorders on the long alkyl chains and a number of positive residual densities remained around the cluster core. These are considered unavoidable due to the nature of the skeleton and measurements. The crystallographic data and a summary of the solution and refinement are given in Table S3. Supplementary crystallographic data of is available from the Cambridge Crystallographic Data Centre as CCDC-2299526.

Alert level B

PLAT241_ALERT_2_B High 'MainMol' Ueq as Compared to Neighbors of C155 Check

PLAT241_ALERT_2_B High 'MainMol' Ueq as Compared to Neighbors of C158 Check

PLAT241_ALERT_2_B High 'MainMol' Ueq as Compared to Neighbors of C160 Check

PLAT241_ALERT_2_B High 'MainMol' Ueq as Compared to Neighbors of C163 Check

PLAT242_ALERT_2_B Low 'MainMol' Ueq as Compared to Neighbors of C159 Check

PLAT242_ALERT_2_B Low 'MainMol' Ueq as Compared to Neighbors of C161 Check

Response: These are derived from the disorders on the octyl substituent. It was difficult to separate

the disordered parts in an appropriate form.

PLAT420_ALERT_2_B D-H Bond Without Acceptor O1 --H1 . Please Check

Response: Phenyl ring (C13-C18) accepts the OH with OH–π interaction.

PLAT910_ALERT_3_B Missing # of FCF Reflection(s) Below Theta(Min). 12 Note

Response: This is probably due to the large unit cell.

PLAT971_ALERT_2_B Check Calcd Resid. Dens. 0.79Ang From Au19 2.60 eA-3

PLAT971_ALERT_2_B Check Calcd Resid. Dens. 0.94Ang From S11 2.55 eA-3

PLAT971_ALERT_2_B Check Calcd Resid. Dens. 0.74Ang From Au20 2.52 eA-3

PLAT973_ALERT_2_B Check Calcd Positive Resid. Density on Au1 1.61 eA-3

PLAT973_ALERT_2_B Check Calcd Positive Resid. Density on Au25 1.56 eA-3

PLAT973_ALERT_2_B Check Calcd Positive Resid. Density on Au6 1.55 eA-3

Response: These are the residual densities near heavy atom core.

Spectroscopic and Spectrometric Measurements. UV–vis–NIR measurements were performed on a V-750 spectrophotometer from JASCO Corporation. The cell length of the quartz cuvette was 10 mm. ^{1}H NMR spectra were measured on JEOL JNM-ECA600 and JNM-ECA400 spectrometers. For ^{1}H NMR measurements, the solvent residual signal was used as the internal standard in acetone-d_6 or THF-d_8. Negative-mode ESI–MS spectra in MeCN were measured on a Solarix-JA spectrometer. The concentration of O_2 was controlled by changing the ratio of bubbled gas of O_2, air and N_2.[7]

Electrochemical Measurements. Cyclic voltammetric and differential pulse voltammetric measurements were carried out in THF containing 0.1 M $TBAPF_6$ as an electrolyte at room temperature under Ar. All measurements were made using a BAS ALS-730E electrochemical analyser with a glassy carbon electrode as a working electrode, a platinum wire as a counter electrode and $Ag/AgNO_3$ as a reference electrode. All redox potentials were determined relative to that of Fc/Fc^+ as 0 V and converted into the redox potential relative to that of SCE.[8]

X-ray absorption fine structure measurements. The Au L_3-edge X-ray absorption fine structure (XAFS) measurements were conducted at beamline BL01B1 of the SPring-8 facility of the Japan Synchrotron Radiation Research Institute (JASRI). The incident X-ray beam was monochromatized by a Si(111) double-crystal monochromator. As a reference, Au foil was measured in transmission mode using ionization chambers at room temperature. XAFS spectra of Au_{25} cluster anions were measured in transmission mode at 10 K using ionization chambers as detectors. The X-ray energies were calibrated using Pt foil. Obtained EXAFS spectra were analysed using the xTunes program.[9] The k^3-weighted EXAFS spectra in the k range 3.0–20.0 $Å^{-1}$ for the Au-L_3 edge were Fourier transformed into r space for structural analysis. The curve-fitting analysis was conducted in the range of 1.5–3.3 Å for the Au-L_3 edge. In the curve-fitting analysis, the phase shifts and backscattering amplitude function of Au–Au, and Au–S were calculated using the FEFF8.5L program.

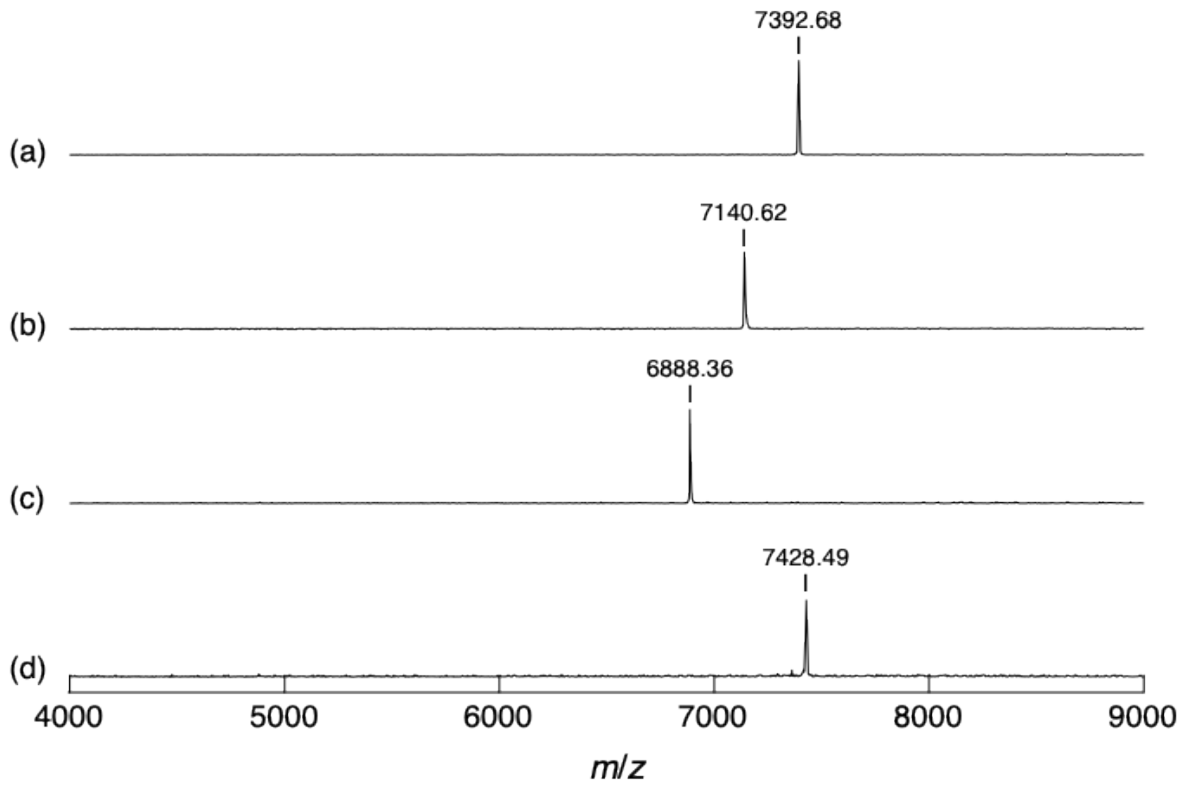

Fig. S1. Negative-mode ESI–MS spectra of **TOA$^+$[Au$_{25}$(SR)$_{18}$]$^-$** in MeCN. **SR** = (a) **SC$_2$Ph** (calcd. *m*/*z* = 7392.90), (b) **SC$_1$Ph** (calcd. *m*/*z* = 7140.66), (c) **SPh** (calcd. *m*/*z* = 6888.38) and (d) **SPhOMe** (calcd. *m*/*z* = 7428.53).

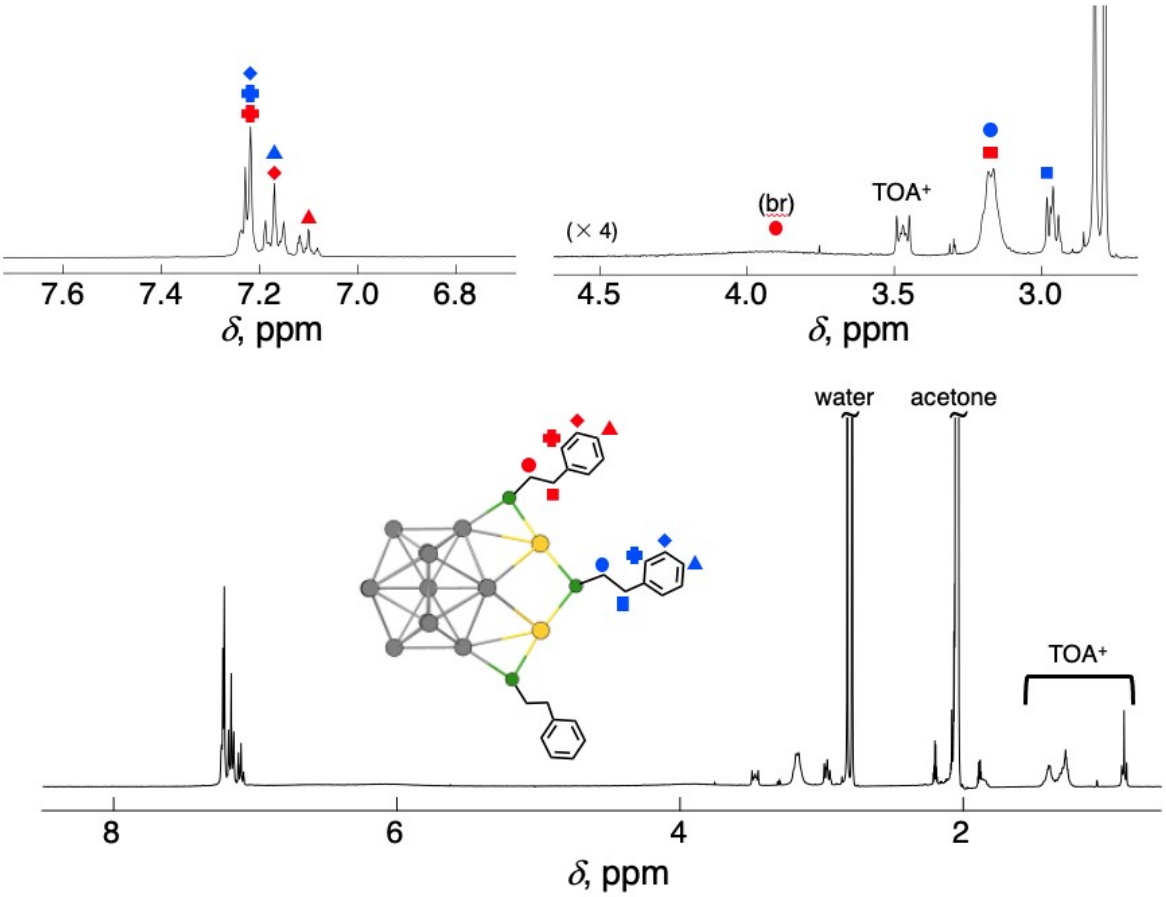

Fig. S2. ^{1}H NMR spectra of **TOA^{+}[Au$_{25}$(SC$_{2}$Ph)$_{18}$]$^{-}$** in acetone-d_6.

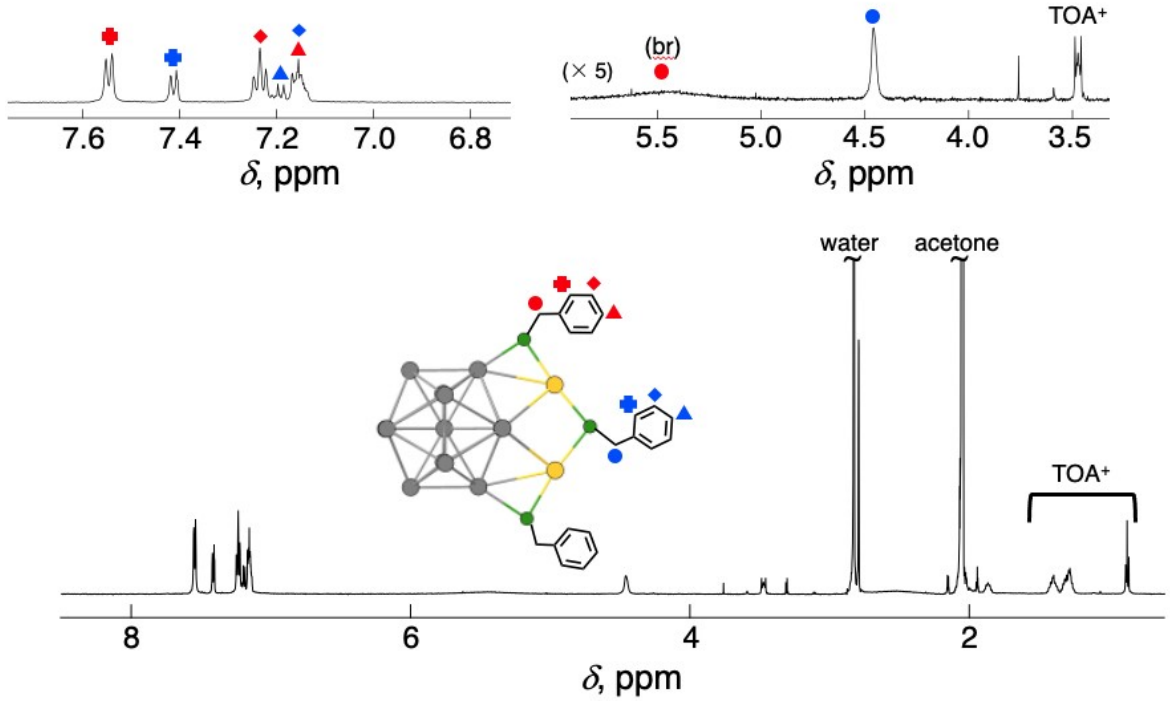

Fig. S3. ^{1}H NMR spectra of **TOA^{+}[Au$_{25}$(SC$_{1}$Ph)$_{18}$]$^{-}$** in acetone-d_6.

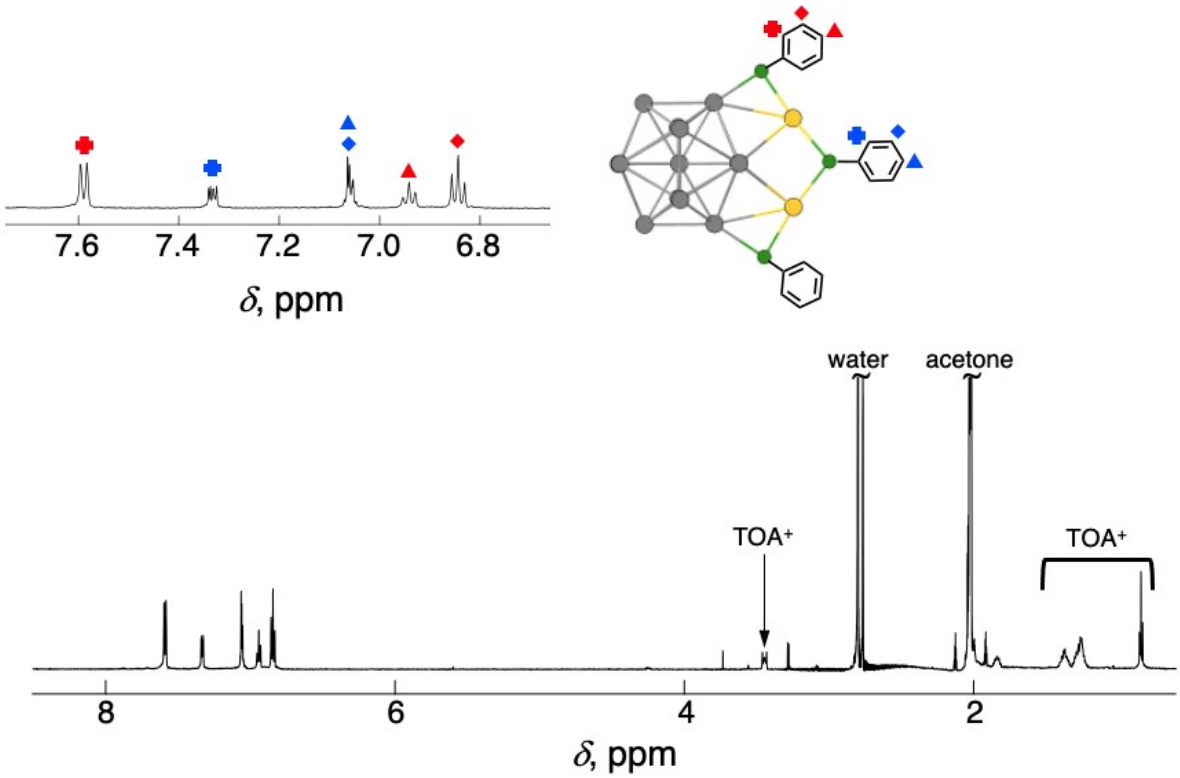

Fig. S4. ^{1}H NMR spectra of **TOA^{+}[Au$_{25}$(SPh)$_{18}$]$^{-}$** in acetone-d_6.

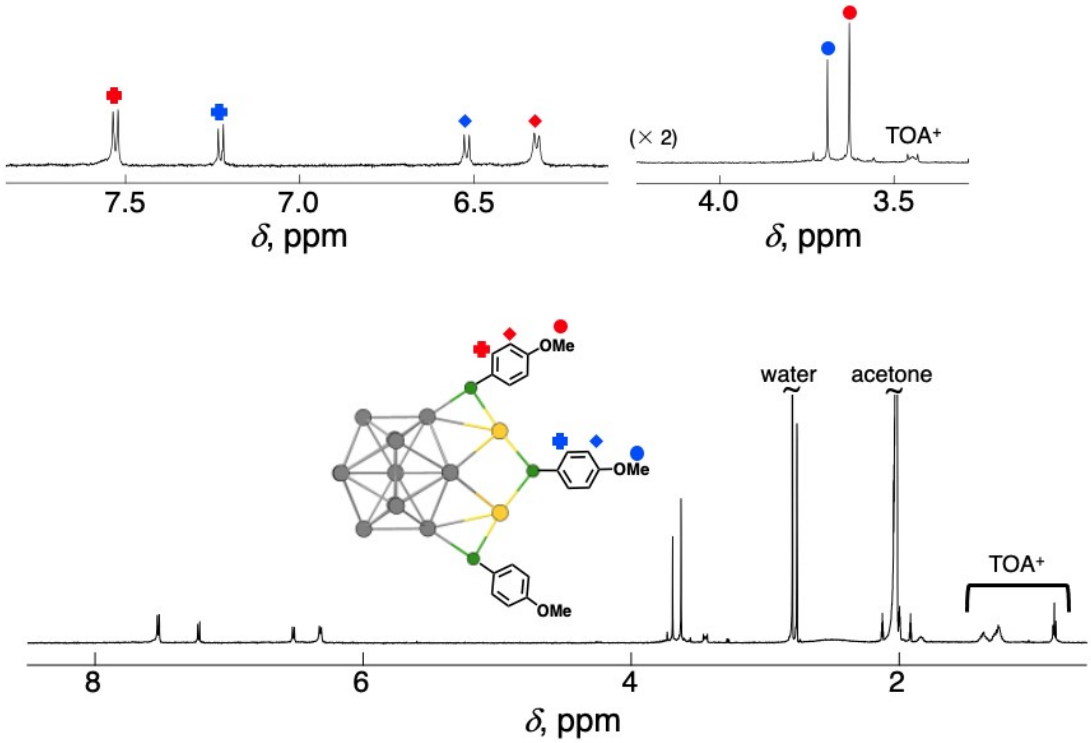

Fig. S5. ^{1}H NMR spectra of **TOA^{+}[Au$_{25}$(SPhOMe)$_{18}$]$^{-}$** in acetone-d_6.

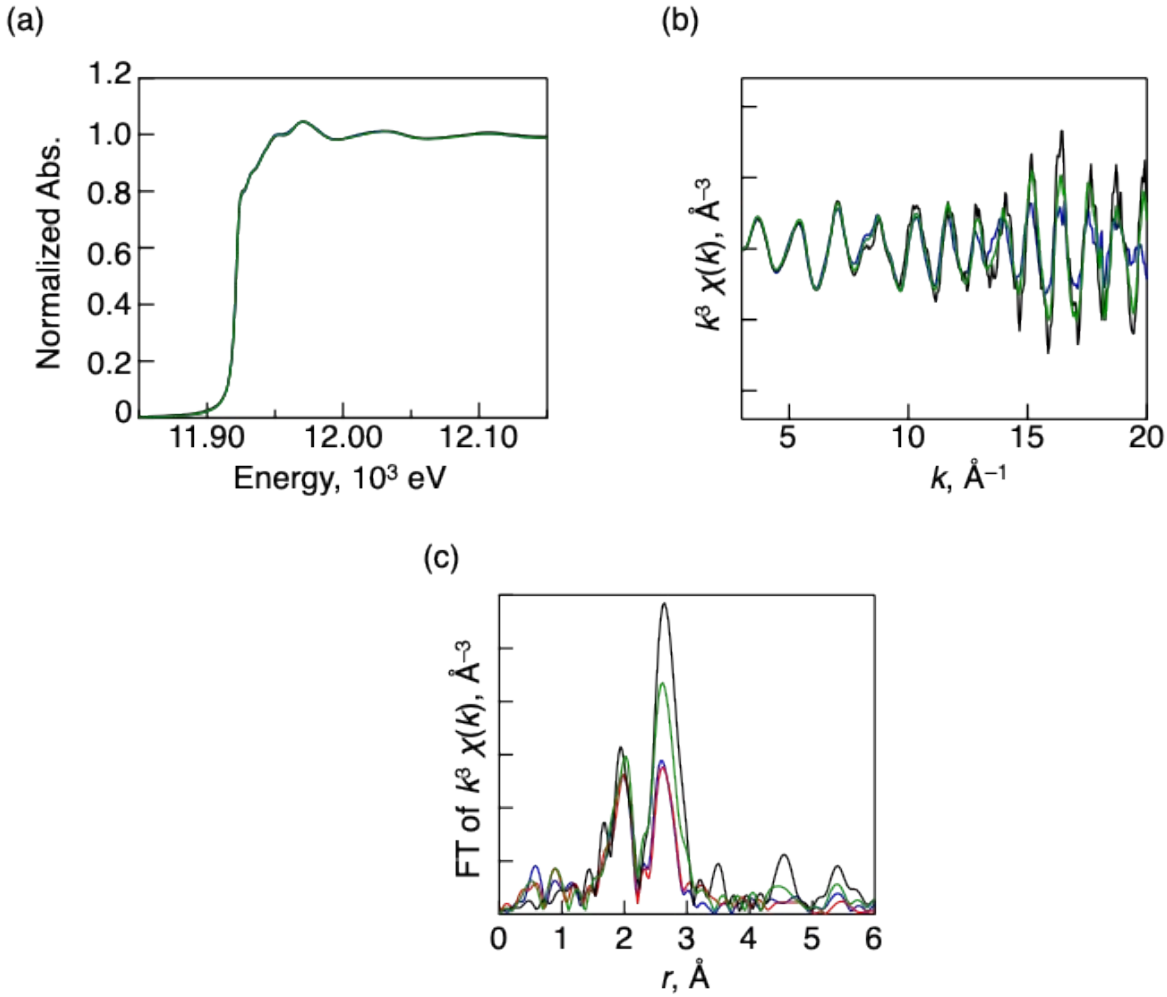

Fig. S6. (a) Au-L_3 edge XANES spectra, (b) EXAFS oscillation, and (c) Fourier-transformed EXAFS spectra of **TOA$^+$[Au$_{25}$(SR)$_{18}$]$^-$**. **SR** = **SC$_2$Ph** (black), **SC$_1$Ph** (green), **SPh** (blue), and **SPhOMe** (red). Spectroscopic measurements were conducted at 10 K in transmission mode. It should be noted that the XANES spectra of **TOA$^+$[Au$_{25}$(SR)$_{18}$]$^-$** were almost overlapped in (a).

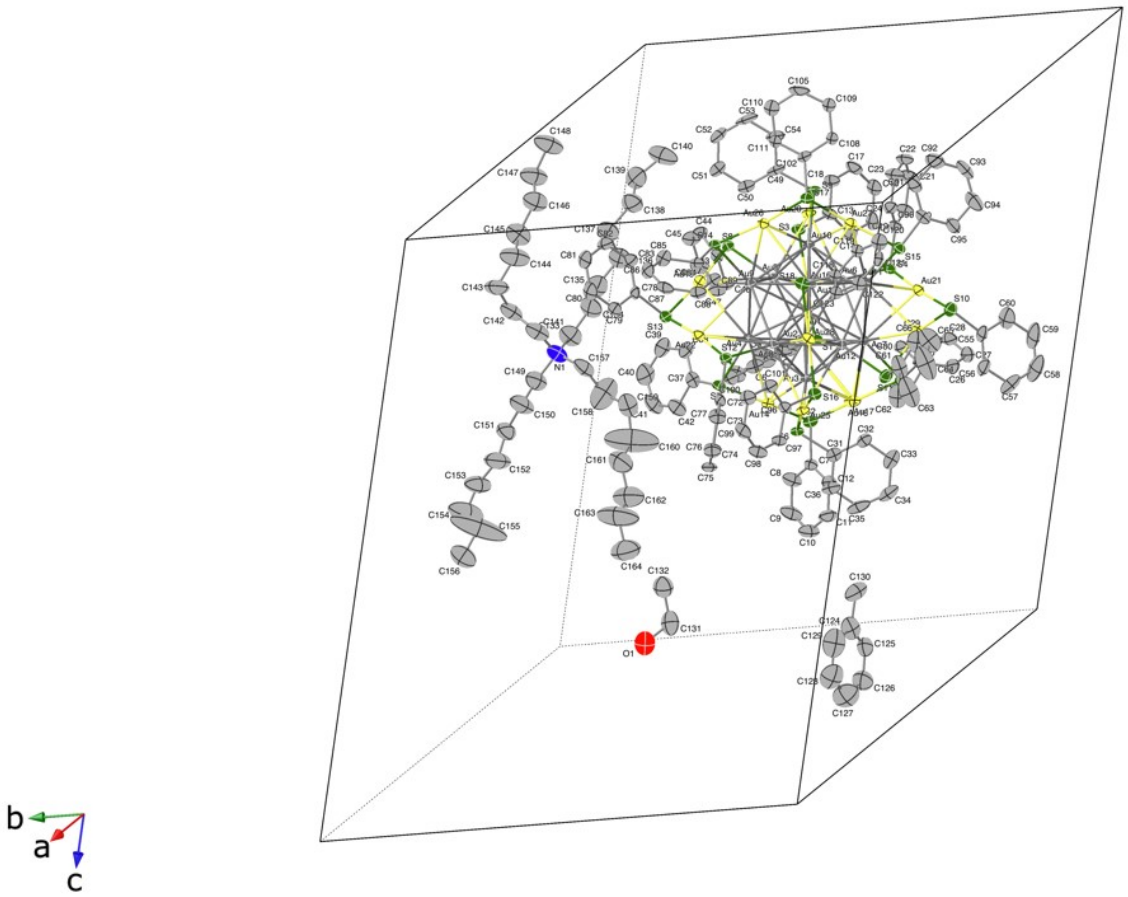

Fig. S7. Unit structure of **TOA$^+$[Au$_{25}$(SPh)$_{18}$]$^-$** with thermal ellipsoids (50% probability). Hydrogen atoms were omitted for clarity.

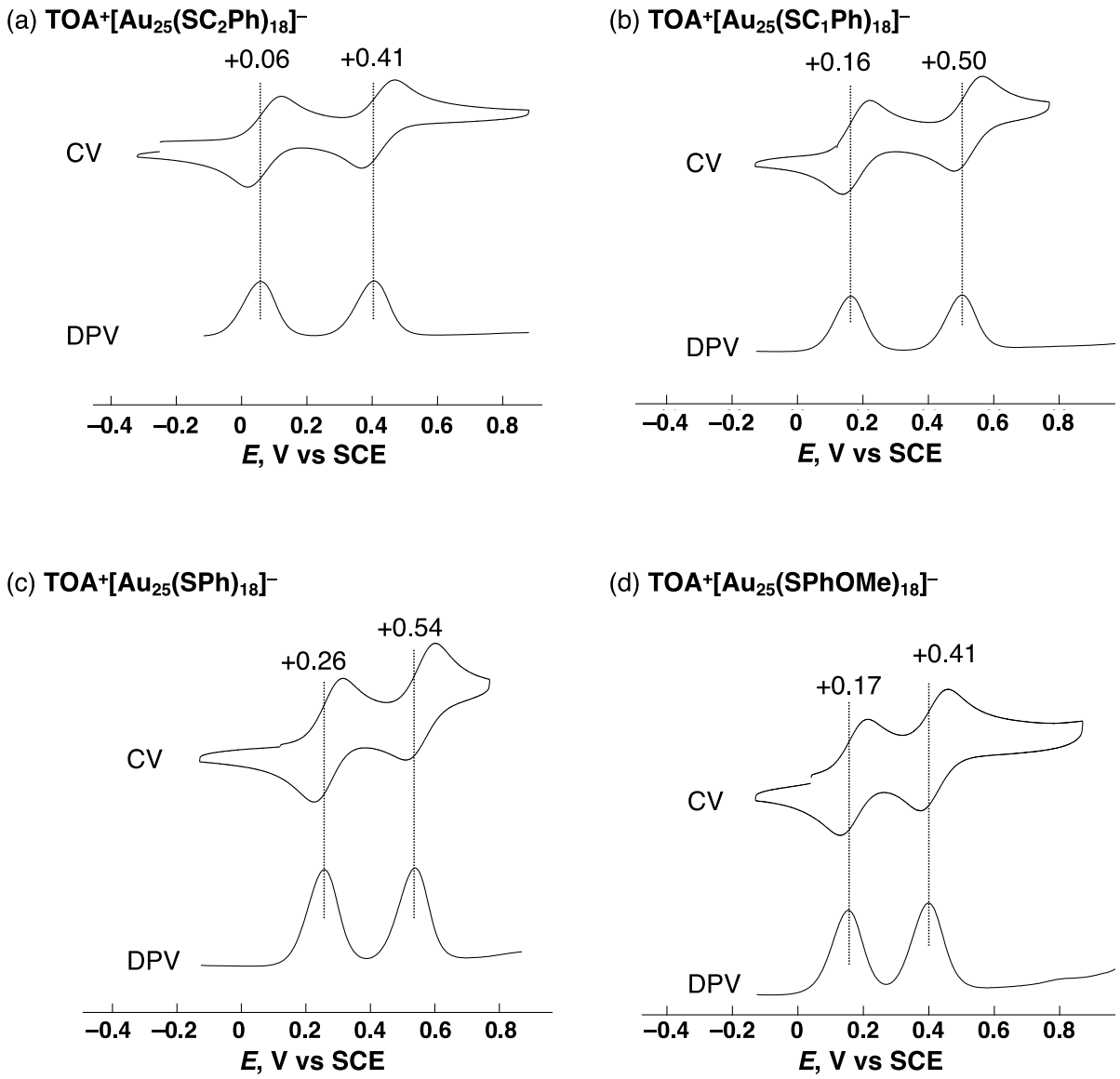

Fig. S8. Cyclic voltammograms (CV) and differential pulse voltammograms (DPV) of **TOA$^+$[Au$_{25}$(SR)$_{18}$]$^-$** in THF containing 0.1 M $TBAPF_6$ as an electrolyte. **SR** = (a) **SC$_2$Ph** (0.26 mM), (b) **SC$_1$Ph** (0.37 mM), (c) **SPh** (0.41 mM) and (d) **SPhOMe** (0.25 mM).

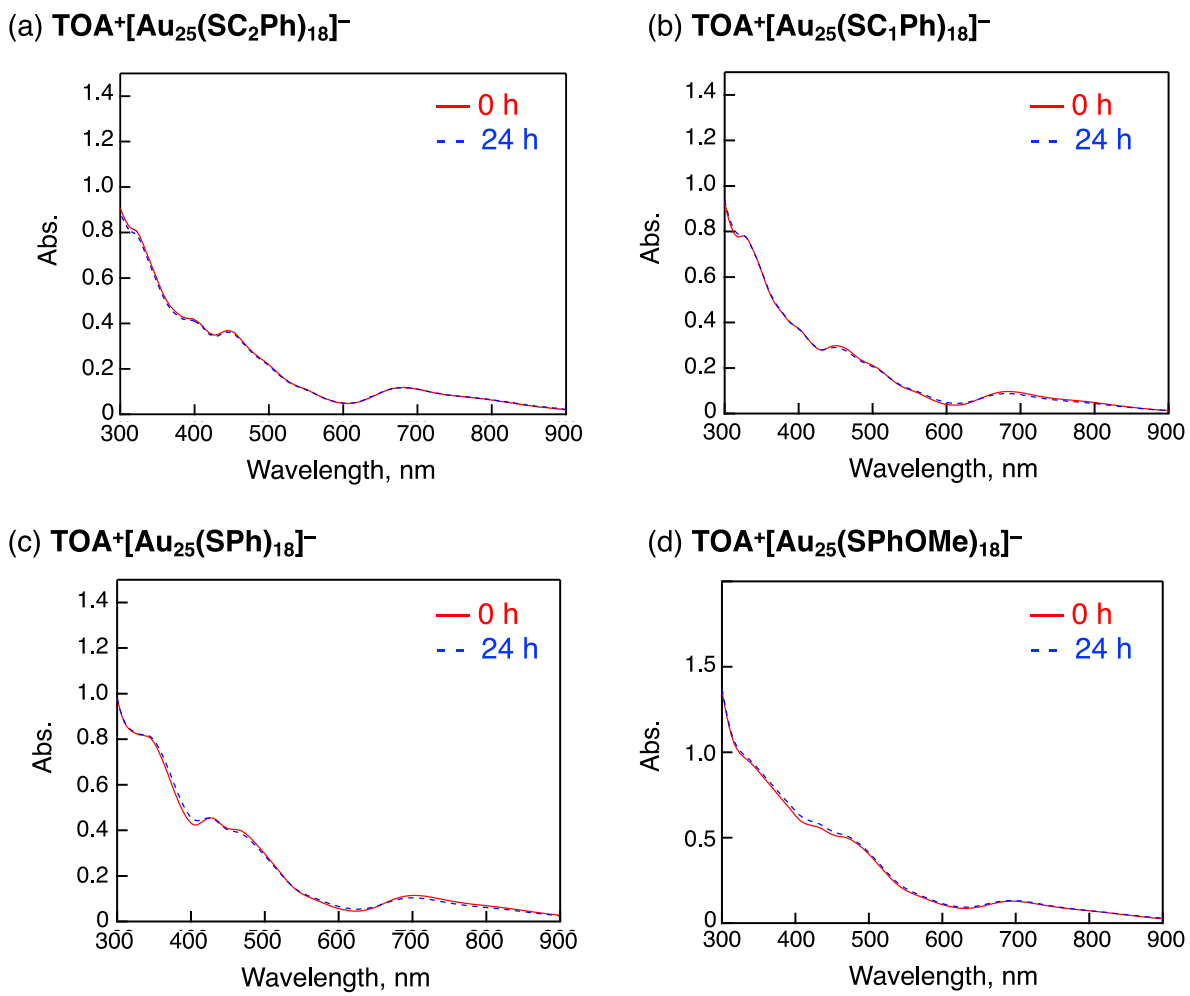

Fig. S9. UV–vis spectral changes of **TOA$^+$[Au$_{25}$(SR)$_{18}$]$^-$** (0.010 mM) in THF under air at 298 K. **SR** = (a) **SC$_2$Ph**, (b) **SC$_1$Ph**, (c) **SPh** and (d) **SPhOMe**.

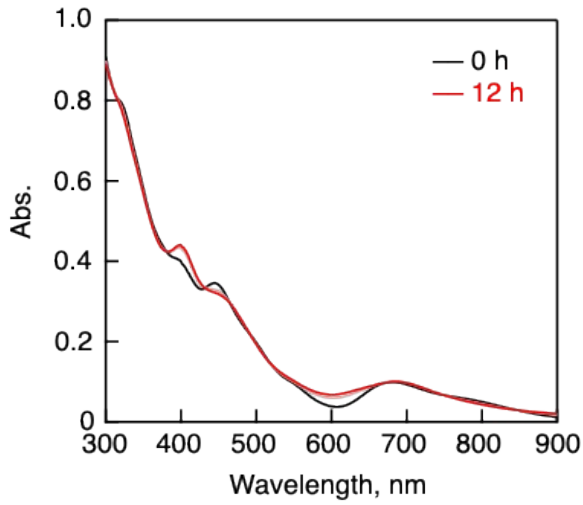

Fig. S10. UV–vis spectral changes of **$TOA^+[Au_{25}(SC_2Ph)_{18}]^-$** (0.010 mM) in THF under air in the presence of TFA (0.050 mM) at 298 K.

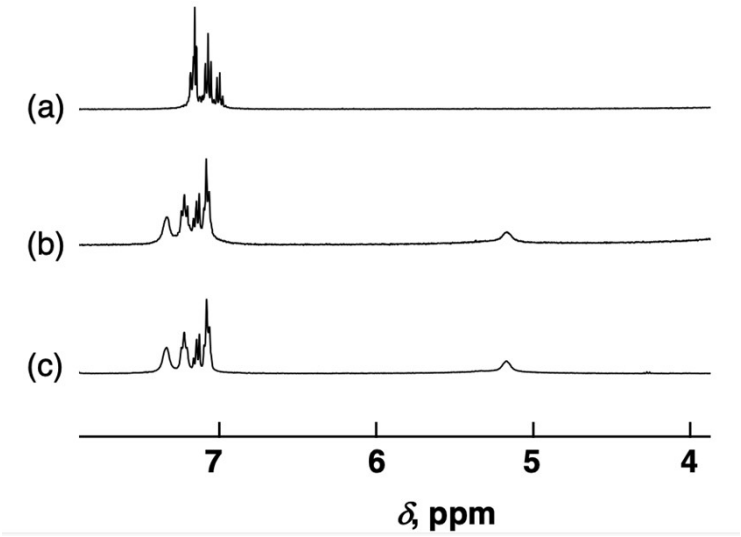

Fig. S11. ^{1}H NMR spectra of (a) **TOA^{+}[Au$_{25}$(SC$_{2}$Ph)$_{18}$]$^{-}$**, (b) **TOA^{+}[Au$_{25}$(SC$_{2}$Ph)$_{18}$]$^{-}$** (0.10 mM) with TFA (2.0 mM) and (c) authentic **[Au$_{25}$(SC$_{2}$Ph)$_{18}$]^{0}** in THF-d_8. **[Au$_{25}$(SC$_{2}$Ph)$_{18}$]^{0}** was prepared according to the previous report. [10]

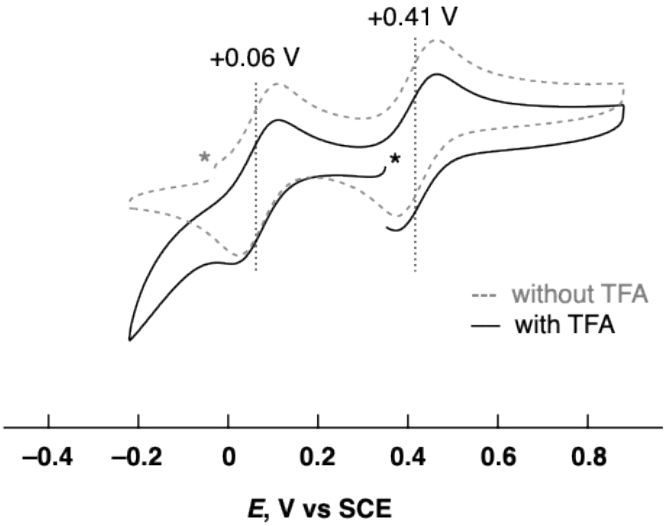

Fig. S12. Comparison of cyclic voltammograms of **$TOA^+[Au_{25}(SC_2Ph)_{18}]^-$** (0.33 mM) with (2.0 mM, solid line) and without TFA (dotted line) in THF containing 0.1 M $TBAPF_6$ as an electrolyte. Asterisks indicate the open circuit potential of each voltammogram.

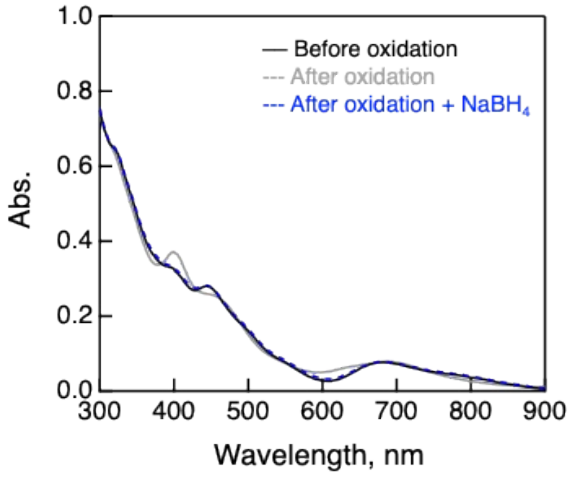

Fig. S13. UV–vis spectra of **TOA$^+$[Au$_{25}$(SC$_2$Ph)$_{18}$]$^-$** (0.010 mM) in THF. Black solid line: before adding TFA; Gray dotted line: after oxidation to form **[Au$_{25}$(SC$_2$Ph)$_{18}$]^0** in the presence of TFA (0.50 mM); Blue dotted line; Addition of $NaBH_4$ to the solution after oxidation reaction of **TOA$^+$[Au$_{25}$(SC$_2$Ph)$_{18}$]$^-$**.

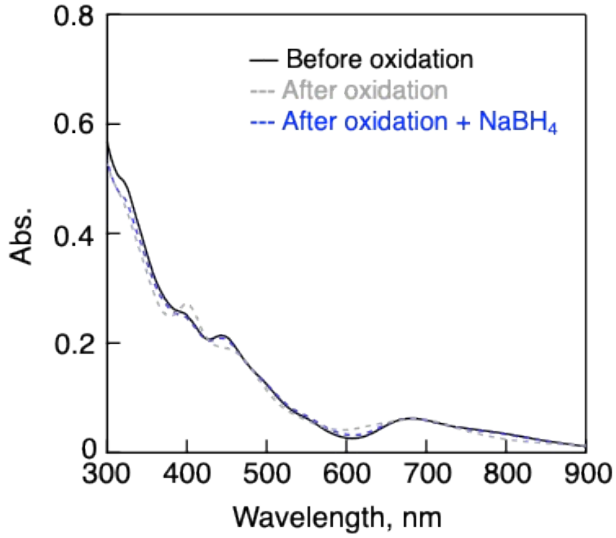

Fig. S14. UV–vis spectra of **TOA$^+$[Au$_{25}$(SC$_2$Ph)$_{18}$]$^-$** (0.010 mM) in THF. Black solid line: before adding TFA; Gray dotted line: after oxidation to form **[Au$_{25}$(SC$_2$Ph)$_{18}$]^0** in the presence of high concentration of TFA (10 mM); Blue dotted line; Addition of $NaBH_4$ to the solution after oxidation reaction of **TOA$^+$[Au$_{25}$(SC$_2$Ph)$_{18}$]$^-$**.

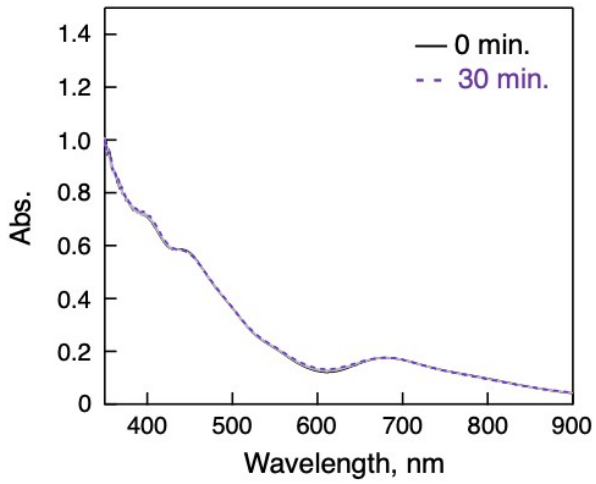

Fig. S15. UV–vis spectral change of **TOA$^+$[Au$_{25}$(SC$_2$Ph)$_{18}$]$^-$** (0.010 mM) in degassed THF in the presence of TFA (0.50 mM).

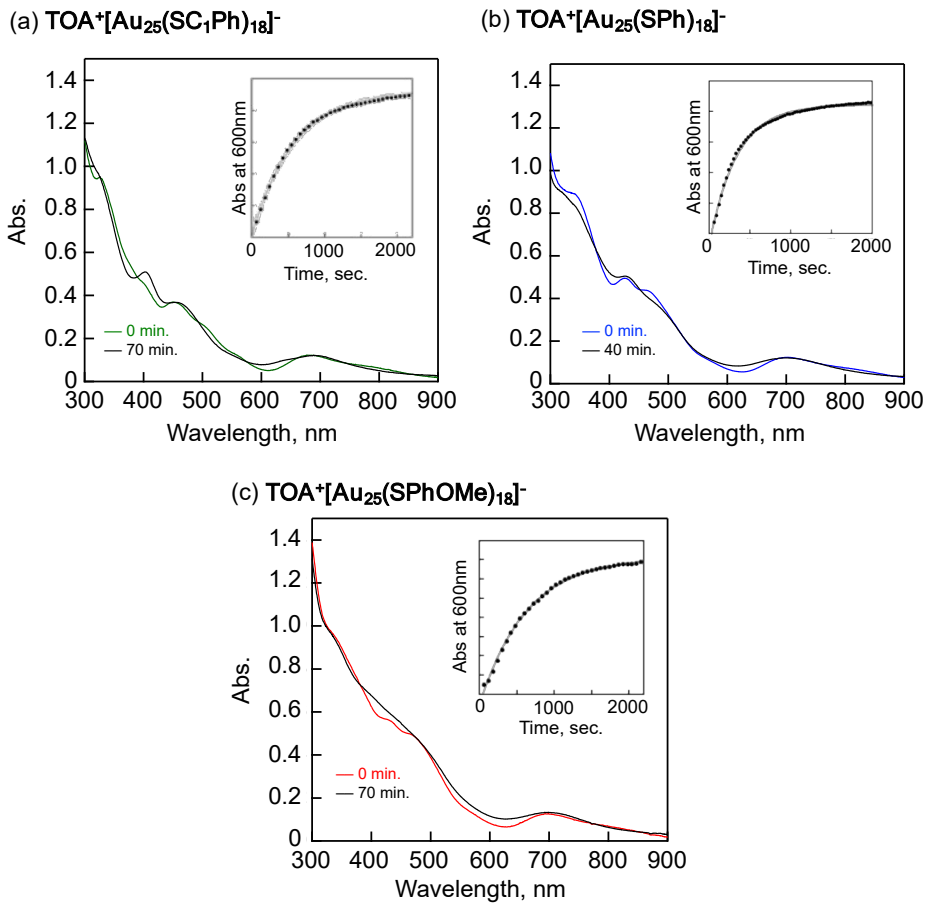

Fig. S16. Time-course UV–vis spectral change of **TOA$^+$[Au$_{25}$(SR)$_{18}$]$^-$** (0.010 mM) in THF containing TFA. Inset: The time profile of absorbance at 600 nm. (a) **TOA$^+$[Au$_{25}$(SC$_1$Ph)$_{18}$]$^-$** with TFA (0.50 mM), (b) **TOA$^+$[Au$_{25}$(SPh)$_{18}$]$^-$** with TFA (2.0 mM) and (c) **TOA$^+$[Au$_{25}$(SPhOMe)$_{18}$]$^-$** (0.50 mM).

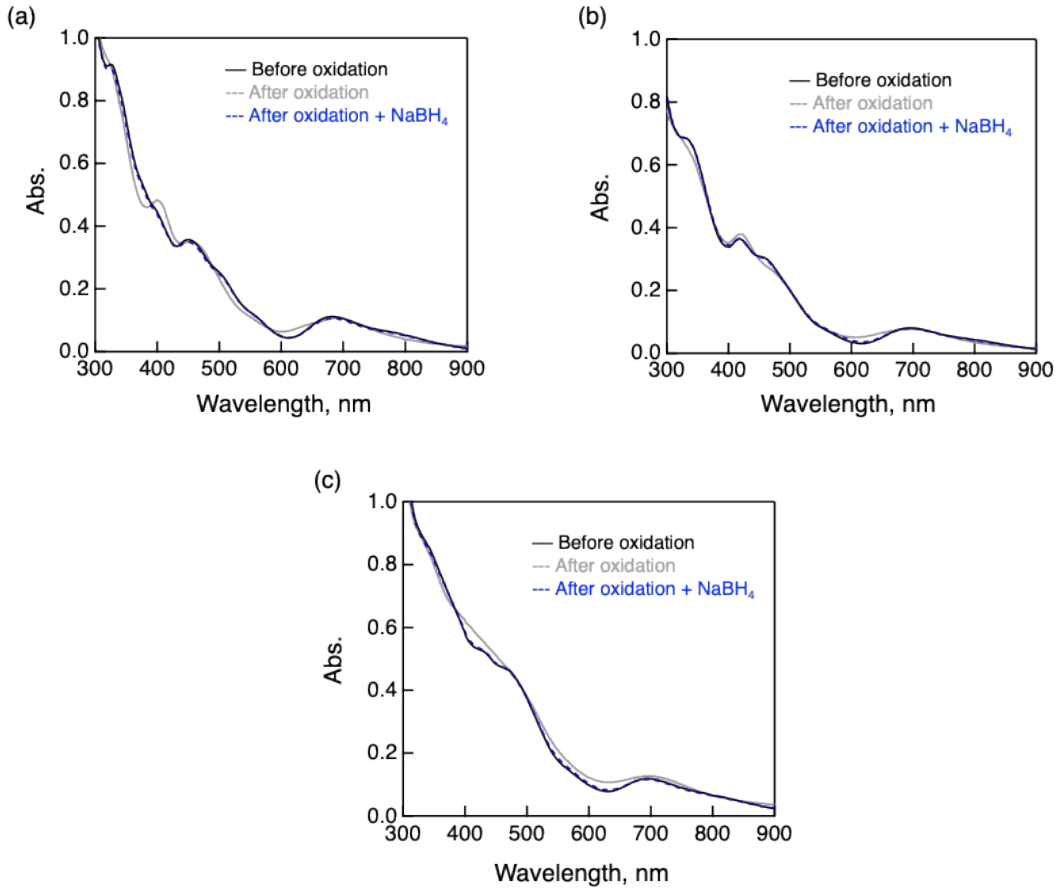

Fig. S17. UV–vis spectra of **TOA**$^{+}$**[Au$_{25}$(SR)$_{18}$]**$^{-}$ (0.010 mM) in THF. **SR** = (a) **SC$_1$Ph**, (b) **SPh**, and (c) **SPhOMe**. Black solid line: before adding TFA; Gray dotted line: after oxidation to form **[Au$_{25}$(SR)$_{18}$]**^{0} in the presence of TFA (0.50 mM); Blue dotted line; Addition of $NaBH_4$ to the solution after oxidation reaction of **TOA**$^{+}$**[Au$_{25}$(SR)$_{18}$]**$^{-}$.

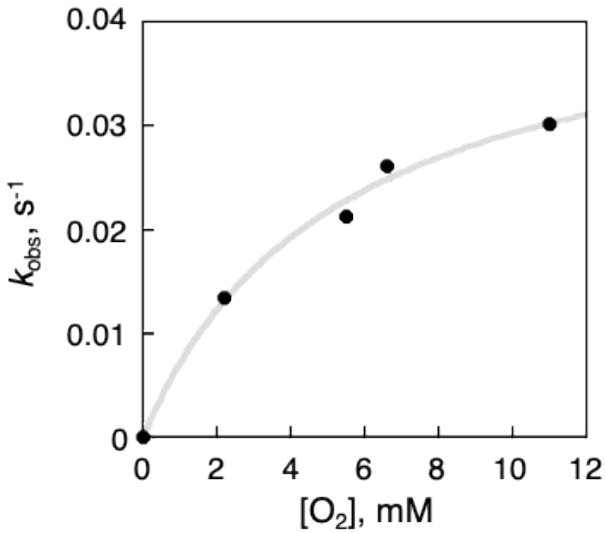

Fig. S18. $[O_2]$ dependence of k_{obs} in the oxidation reaction of **TOA$^+$[Au$_{25}$(SC$_2$Ph)$_{18}$]$^-$** in THF ([TFA] = 2.0 mM) at 298 K.

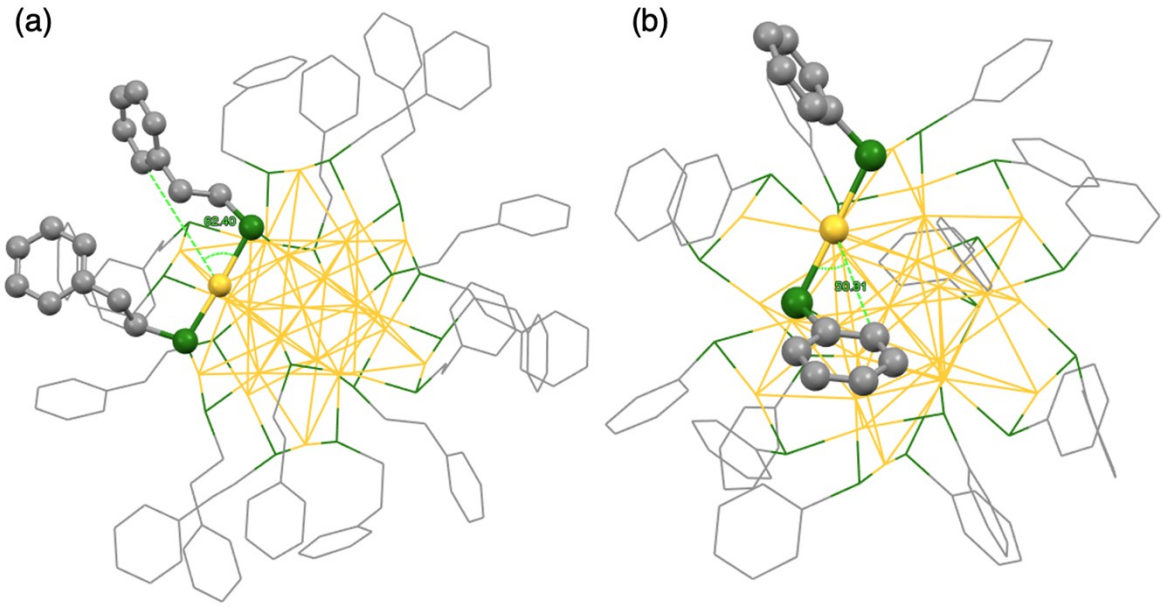

Fig. S19. Representative cone half angle of (a) **[Au$_{25}$(SC$_2$Ph)$_{18}$]**$^-$ and (b) **[Au$_{25}$(SPh)$_{18}$]**$^-$. Protons were omitted for clarity. The half cone angles (θ) were calculated as the averaged values of 24 C-Au-S angles in single crystallographic data of **[Au$_{25}$(SR)$_{18}$]**$^-$. Atom labels: Yellow: gold, Green: sulfur, Light grey: carbon.

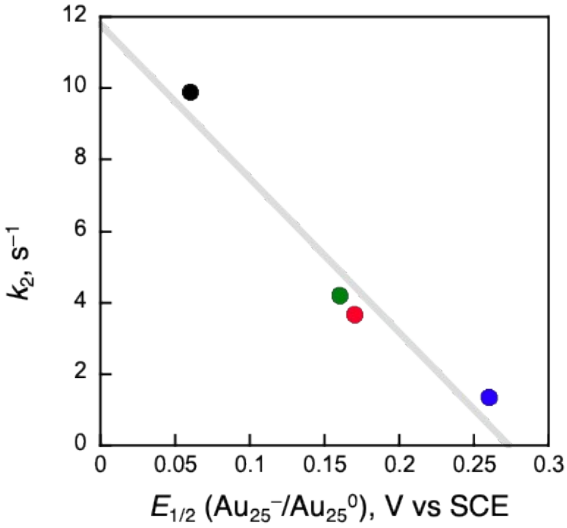

Fig. S20. Plot of rate constants (k_2) against the first redox potentials ($E_{1/2}$ (Au_{25}^-/Au_{25}^0)) of **$TOA^+[Au_{25}(SR)_{18}]^-$**. **SR** = **$SC_2Ph$** (black), **$SC_1Ph$** (green), **SPhOMe** (red) and **SPh** (blue).

Table S1. Structural parameters of **TOA$^+$[Au$_{25}$(SR)$_{18}$]$^-$** obtained by curve-fitting analysis of Au L_3-edge EXAFS spectra.

$[Au_{25}(SR)_{18}]^-$	Bond	*CN*	*r*, Å	DW (σ^2), Å^2	*R*, %
$[Au_{25}(SC_2Ph)_{18}]^-$	Au-S	1.40(18)	2.31(3)	0.0030(24)	13.7
	Au-Au	1.63(15)	2.78(2)	0.0031(13)	
	Au-Au	1.27(17)	2.94(2)	0.0035(18)	
$[Au_{25}(SC_1Ph)_{18}]^-$	Au-S	1.40(18)	2.32(3)	0.0030(23)	14.7
	Au-Au	1.59(15)	2.78(2)	0.0030(13)	
	Au-Au	1.2(2)	2.92(3)	0.0042(23)	
$[Au_{25}(SPh)_{18}]^-$	Au-S	1.39(19)	2.31(3)	0.0036(28)	10.4
	Au-Au	1.54(17)	2.78(2)	0.0037(16)	
	Au-Au	1.2(2)	2.89(5)	0.0064(39)	
$[Au_{25}(SPhOMe)_{18}]^-$	Au-S	1.36(19)	2.32(3)	0.0036(28)	12.3
	Au-Au	1.75(18)	2.79(2)	0.0038(16)	
	Au-Au	1.2(2)	2.90(4)	0.0053(30)	

Table S2. Comparison of structural parameters of **TOA$^+$[Au$_{25}$(SPh)$_{18}$]$^-$** obtained by single-crystal X-ray diffraction analysis with previously reported **TOA$^+$[Au$_{25}$(SC$_2$Ph)$_{18}$]$^-$** [11]

	TOA$^+$[Au$_{25}$(SC$_2$Ph)$_{18}$]$^-$	**TOA$^+$[Au$_{25}$(SPh)$_{18}$]$^-$**
Au-Au$_{core}$, Å	2.776	2.782
Au-Au$_{surface}$, Å	2.919	2.926
Au$_{staple}$-S$_{core}$, Å Au$_{staple}$-S$_{apex}$, Å	2.30	2.30
Au$_{surface}$-S$_{core}$, Å	2.39	2.40

The bond distances are described as averaged values.

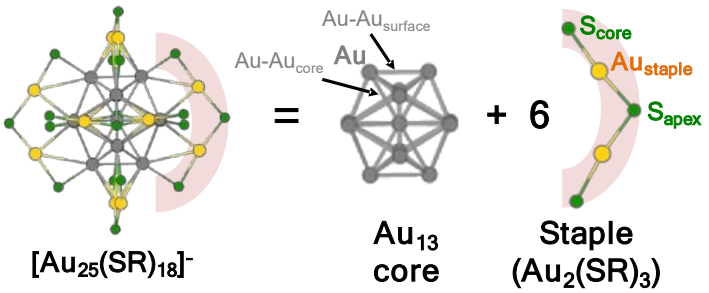

Table S3. X-ray crystallographic data for **TOA$^+$[Au$_{25}$(SPh)$_{18}$]$^-$**.

crystal system	Triclinic
space group	$P\bar{1}$ (#2)
T, K	90(2)
formula	$C_{147.35}H_{170.12}Au_{25}NOS_{18}$
FW	7472.46
a, Å	17.0841(8)
b, Å	20.5511(10)
c, Å	26.5333(12)
α, deg	73.391(2)
β, deg	72.258(2)
γ, deg	65.634(2)
V, Å^3	7943.6(7)
Z	2
λ, Å	0.71073 (Mo Kα)
D_c, g cm^{-3}	3.124
reflns measured	193152
reflns unique	36399
R_1 ($I > 2\sigma(I)$)	0.0306
wR_2 (all)	0.0704
GOF	1.034

References

1. J. F. Parker, J. E. F. Weaver, F. McCallum, C. A. Fields-Zinna, R. W. Murray, *Langmuir*, 2010, **26**(16), 13650-13654.
2. A. Das, T. Li, K. Nobusada, C. Zeng, N. L. Rosi, R. Jin, *J. Am. Chem. Soc.,* 2013, **135**(49), 18264-18267.
3. G. M. Sheldrick, *Acta Cryst.,* 2015, **A71**, 3.
4. G. M. Sheldrick, *Acta Cryst.,* 2015, **C71**, 3.
5. C. Kabuto, S. Akine, S. E. Kwon, *J. Cryst. Soc. Jpn.,* 2009, **51**, 218.
6. O. V. Dolomanov, L. J. Bourhis, R. J. Gildea, J. A. K. Howard, H. Puschmann, *J. Appl. Cryst.* 2009, **42**, 339.
7. W. Suzuki, H. Kotani, T. Ishizuka, T. Kojima, *J. Am. Chem. Soc.* 2019, **141**, 5987-5994.
8. N. G. Connelly, W. E. Geiger, *Chem. Rev.* 1996, **96**, 877-910.
9. H. Asakura, S. Yamazoe, T. Misumi, A. Fujita, T. Tsukuda, T. Tanaka, *Radiat. Phys. Chem.,* 2020, **175**, 108270.
10. M. A. Tofanelli, K. Salorinne, T. W. Ni, S. Malola, B. Newell, B. Phillips, H. Häkkinen, C. J. Ackerson, *Chem. Sci.* 2016, **7**, 1882.
11. M. Zhu, C. M. Aikens, F. J. Hollander, G. C. Schatz, R. Jin, *J. Am. Chem. Soc.,* 2008, **130**, 5883-5885.